Electronic Supplementary Information for "The compression of a heavy floating elastic film"

Etienne Jambon-Puillet[a], Dominic Vella[a,b], Suzie Protière[a]

1 Model of the floating heavy film prior to self-contact

We consider an incompressible film of length L_0, width W, thickness t and density ρ_s lying between a fluid of density ρ_{up} (for the upper fluid) and a lower liquid of density $\rho_{low} > \rho_{up}$. The film is compressed uniaxially in the x direction (see Fig. 1). We introduce the intrinsic coordinates (s, θ) in which s is the arclength and $\theta(s)$ is the local angle between the tangent and the horizontal axis x; we parametrize the film centreline in terms of arc-length, $[x(s), y(s)]$.

Neglecting surface tension, the energy of this system is: $U = U_b + U_{low} + U_{up} + U_g$ with U_b the bending energy, U_{low} and U_{up} the gravitational potential energies of the liquid/fluids that are displaced by the film and U_g the gravitational energy of the film itself. In our system of coordinates we have:

$$U_b = \frac{BW}{2}\int_{-L_0/2}^{L_0/2} (\partial_s\theta)^2 \,\mathrm{d}s$$
$$U_{low} + U_{up} = \frac{\Delta\rho g W}{2}\int_{-L_0/2}^{L_0/2} y(s)^2\cos\theta \,\mathrm{d}s$$
$$U_g = (\rho_s - \rho_{low})gWt\int_{-L_0/2}^{L_0/2} y(s)\,\mathrm{d}s$$

with g the gravitational acceleration, $\Delta\rho = \rho_{low} - \rho_{up}$ the density difference between the fluids, B the bending modulus (per unit width) of the beam, $B = Et^3/[12(1-\nu^2)]$, E is the Young's modulus and ν the Poisson ratio. Assuming the film is inextensible, we have a global constraint on the end displacement:

$$\Delta = L_0 - L = \int_{-L_0/2}^{L_0/2}(1-\cos\theta)\,\mathrm{d}s$$

We also have a local constraint due to the use of intrinsic coordinates $\partial_s y(s) = \sin\theta(s)$.

To determine the equilibrium profile of the compressed film, we first minimize the total energy accounting for the two constraints mentioned above. This adds two Lagrange multipliers: P for the end displacement (which corresponds physically to the compressive force applied, $P = \partial_\Delta U$) and $Q(s)$ for the relation between $\partial_s y$ and θ. To facilitate the calculation, we rescale lengths by $\ell_{eh} = (B/\Delta\rho g)^{1/4}$, energy by WB/ℓ_{eh} and P by $W(B\Delta\rho g)^{1/2}$ and only use dimensionless quantities in the following. We find that the energies are

$$U_b = \frac{1}{2}\int_{-L_0/2}^{L_0/2}(\partial_s\theta)^2\,\mathrm{d}s, \quad U_{low}+U_{up} = \frac{1}{2}\int_{-L_0/2}^{L_0/2} y(s)^2\cos\theta\,\mathrm{d}s, \quad U_g = M\int_{-L_0/2}^{L_0/2} y(s)\,\mathrm{d}s$$

[a] *Institut Jean le Rond d'Alembert, UPMC Paris 6, CNRS UMR 7190, 4 Pl Jussieu, 75005, Paris, France*
[b] *Mathematical Institute, Andrew Wiles Building, University of Oxford, Woodstock Rd, Oxford, OX2 6GG, UK*

In this process a dimensionless number appears,

$$M = \frac{(\rho_s - \rho_{low})t}{\Delta\rho\ell_{eh}},$$

which measures the weight of the film relative to the restoring force provided by Archimedes' buoyancy over the horizontal length ℓ_{eh}. The action to minimize is therefore $\mathcal{S} = \int_{-L_0/2}^{L_0/2} \mathrm{d}s\, \mathcal{L}(\theta,\, \partial_s\theta,\, y,\, \partial_s y)$ with

$$\mathcal{L} = \tfrac{1}{2}\left(\partial_s\theta\right)^2 + \tfrac{1}{2}y^2\cos\theta + My - P(1-\cos\theta) - Q(s)(\sin\theta - \partial_s y)$$

We use Hamiltonian mechanics, following Diamant and Witten[1], to perform the minimization. The conjugate momenta and the Hamiltonian are:

$$p_\theta = \tfrac{\partial\mathcal{L}}{\partial(\partial_s\theta)} = \partial_s\theta, \quad p_y = \tfrac{\partial\mathcal{L}}{\partial(\partial_s y)} = Q$$
$$\mathcal{H} = p_\theta\partial_s\theta + p_y\partial_s y - \mathcal{L}$$

Since $\mathcal{L}$ has no explicit dependence on s, $\mathcal{H}$ is a constant of motion, thus $\mathcal{H}(s) = \mathcal{H}(\pm L_0/2)$. Here we focus on localized deformations and therefore choose the boundary conditions

$$y(\pm L_0/2) = \theta(\pm L_0/2) = \partial_s\theta(\pm L_0/2) = 0,$$

which immediately gives that $\mathcal{H}(s) = 0$, i.e.

$$\mathcal{H} = \tfrac{1}{2}\left(\partial_s\theta\right)^2 + Q\sin\theta - \tfrac{1}{2}y^2\cos\theta - My + P(1-\cos\theta) = 0 \tag{1}$$

Hamilton's equations $\partial_s p_\theta = -\partial\mathcal{H}/\partial\theta$ and $\partial_s p_y = -\partial\mathcal{H}/\partial y$ then give:

$$\partial_s^2\theta + \left(\tfrac{1}{2}y^2 + P\right)\sin\theta + Q\cos\theta = 0 \tag{2}$$
$$\partial_s Q - y\cos\theta - M = 0 \tag{3}$$

If we differentiate (2) with respect to s and eliminate $Q\sin\theta$ with (1) and $\partial_s Q$ with (3) we get:

$$\partial_s^3\theta + \left[\tfrac{1}{2}\left(\partial_s\theta\right)^2 + P\right]\partial_s\theta + y(1 - M\partial_s\theta) + M\cos\theta = 0 \tag{4}$$

This equation can be solved numerically to obtain the profile of the film.

To compare (4) with the final equation of Diamant and Witten[1], we differentiate with respect to s:

$$\partial_s^4\theta + \partial_s^2\theta\left[\tfrac{3}{2}\left(\partial_s\theta\right)^2 + P - My\right] + \sin\theta(1 - 2M\partial_s\theta) = 0 \tag{5}$$

When $M = 0$, equation (5) reduces to that derived by Diamant and Witten[1].

Remark (Boundary conditions). To model our experiments, the appropriate boundary conditions are $y(\pm L_0/2) = 0$. However, for an idealized, infinite film the boundary condition $y(\pm\infty) = -M$ might be more appropriate (so that it is freely floating far from the localization). This modification would change one term in the final equation, however this term can be absorbed through a shift in the load[2] to recover equation (5).

2 Fold symmetries

Pocivavsek *et al*[3] identify four possible buckling modes (two symmetric and two antisymmetric ones). Experimentally they observe that at high compression all their films become symmetric (mainly downward) but give no explanation for this phenomenon. Theoretical works on weightless infinite films[4,5] show that there are an infinity of continuous buckling modes from symmetric to antisymmetric which all have the same energy. Rivetti and Neukirch[6] study finite length films numerically and show that, depending on the film length, there is one stable buckling mode

for a given compression. In a numerical experiment in which the compression is increased gradually, the film can transition from antisymmetric to symmetric (and vice versa) configurations several times via non symmetric modes. They call this the branching route. In our experiments we observe such transitions (Fig. S1). Two possible branching routes are observed: the wrinkles start symmetric and the fold remains symmetric until self-contact or the wrinkles start antisymmetric (or non symmetric) and the film goes through a series of non symmetric modes until it reaches a downward symmetric fold and then stays downward symmetric until self-contact. We never observe more than one transition, even though multiple transitions have been predicted theoretically. At high compression, the film weight (neglected in previous theoretical work) stabilizes the downward symmetric configuration, making it energetically favourable over other modes.

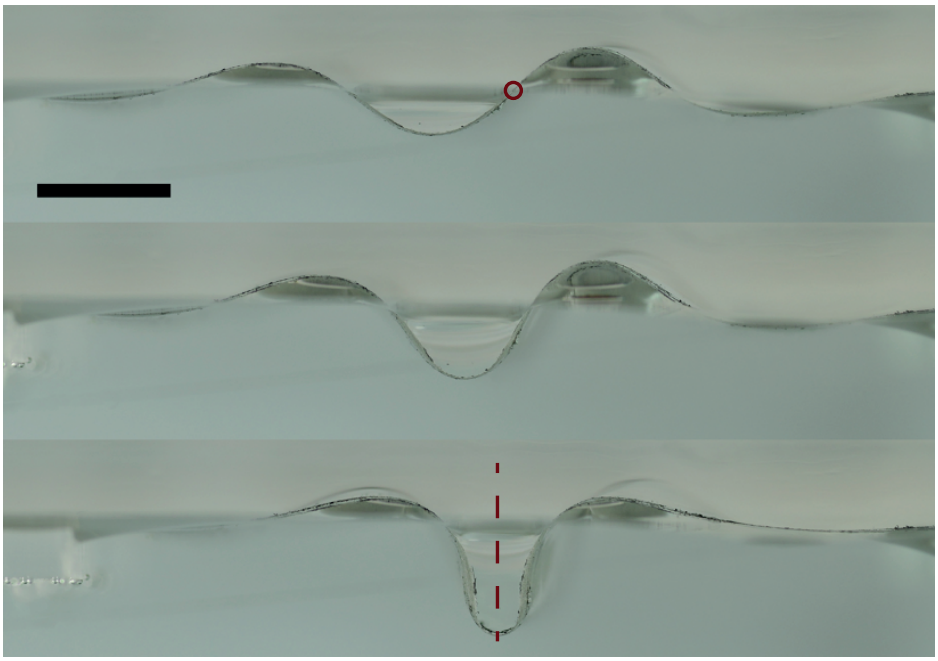

Figure S1: Side pictures of an elastic film at the oil/water interface, illustrating the buckling route ($\rho_s = 1.4$ g cm^{-3}, $M = 0.10$, shown by the orange curves in Fig. 3 of the main text). Top picture: antisymmetric (centre of rotation highlighted), middle picture: no symmetry and bottom picture: symmetric (reflection axis drawn). Compression increases from top to bottom with $\Delta/\lambda = 0.20$, 0.33, 0.49, respectively. Scale bar: 5mm.

Finally, the initial state of the film is very sensitive to the boundary conditions: if the film is not perfectly aligned, the symmetry of the profile and the fold position are noticeably modified. Moreover, small defects (in the thickness or material properties) can modify the buckling modes making prediction of the precise buckling route in a practical application difficult.

3 Role of surface tension

Surface tension is neglected in most works on floating thin films since this assumption allows the problem to be simplified to a two dimensional analysis. Nevertheless, small capillary bridges exist at the edges of the film which exert strong forces on it. For example, it has been shown[7] that for ultrathin films with very low bending modulus, surface tension modifies the wrinkle wavelength over a distance $\ell_c = (\gamma/\Delta\rho g)^{1/2}$. For the effect of surface tension to be negligible, therefore, the film needs to have a high bending modulus (such that $\ell_{eh} \gg \ell_c$). In the experiments presented in this paper surface tension effects are small but visible: we find a slight reduction of the wavelength (about 15%) at the edges, with the film profiles distorted in the neighbourhood of the edge; finally, self-contact is reached sooner (i.e. at smaller compressions).

To highlight the effect of surface tension in this region, we take relatively transparent films (thin pure VPS films and polydimethylsiloxane or PDMS films) with negligible weight ($M \sim 0$) and draw lines with a marker pen away from the edges. Since the films are transparent, we can focus the camera on the drawn line. Fig. S2 (a) shows that the profile far from the edge, and hence undisturbed by surface tension, is well fitted by the usual solution [4,5]. However, the profile at the edge of the film, where surface tension creates strong deformations, cannot be fitted by such solutions. Fig. S2 (b) shows that the teardrop shape at self-contact is accurately predicted with the solution from [4,5] only far from the film edges.

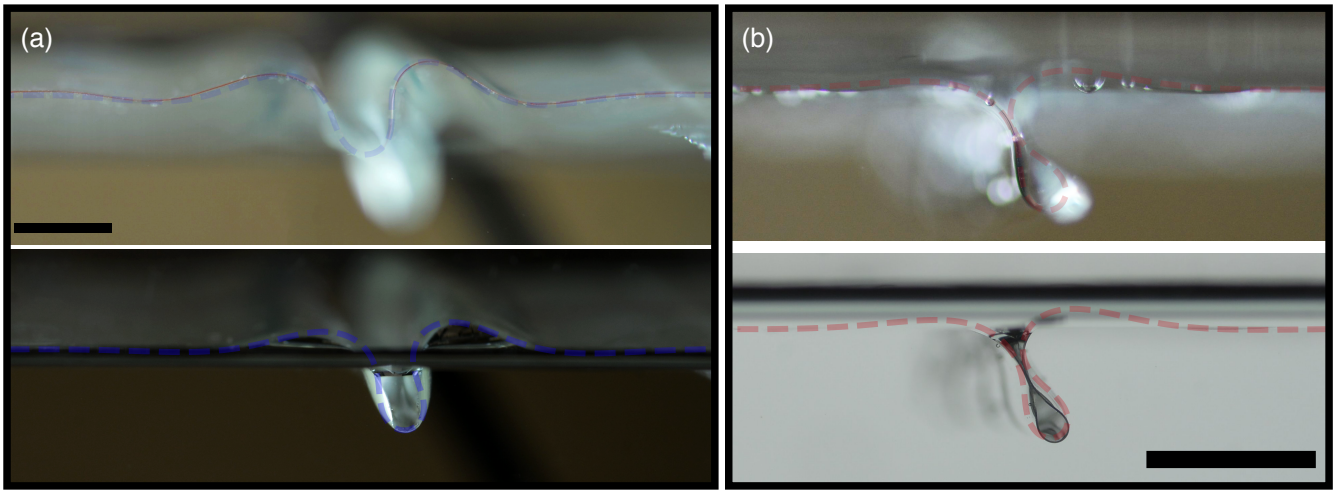

Figure S2: **(a)** Side picture of a VPS film compressed at the air/water interface viewed in the centre of the film (top) and at the edge of the film (bottom), both with the same compression. Top picture: the camera is focused on the centre of the film. The red line is physically drawn on the film, while the overlaid blue dashed curve is the theoretical solution with the experimentally measured parameters (Δ, λ) and $k\phi = 0.60$. Bottom picture: the camera is focus on the edge of the film, the overlaid blue dashed line is the theoretical solution with the experimentally measured parameters with $k\phi = 0.35$. **(b)** Side images of a PDMS film compressed at the air/water interface viewed at the point of self-contact (though not the same value of Δ in each case); here images are shown with the camera focussed ~ 8 mm from the edge and at the edge. Top picture: focus is on the centre of the film. The black line is physically drawn on the film while the overlaid red dashed curve is the theoretical solution with the experimental parameters and $k\phi = 0.45$. Bottom picture: focus is at the edge, the overlaid red dashed line is the theoretical solution with the experimental parameters and $k\phi = 0.45$. Scale bars: 5 mm.

4 Heavy hanging column model after self-contact

A vertical film of length L^*, thickness t, width W and density ρ_s is immersed in water ρ_w. The film is clamped at the top and a vertical force F is pushing at the bottom along the full width W. We introduce the intrinsic coordinates (s, θ) where s is the arclength going from bottom to top and $\theta(s)$ is the local angle between the tangent and the vertical axis x (schematic Fig. 6). The (x, y) coordinates are therefore rotated clockwise by 90 degrees compared to those used for prior to contact. We parametrize the film centreline as $[x(s), y(s)]$ which are given in terms of the intrinsic coordinates by $(\partial_s x = -\cos\theta, \partial_s y = -\sin\theta)$. The problem is invariant along the width of the film so we can eliminate W and consider the problem in two dimensions. The internal forces, $n_x(s)$ and $n_y(s)$ and moment equilibrium, $\overrightarrow{m(s)} = m(s)\vec{e_z}$ per unit of width on a small portion of the beam read as:

$$\partial_s n_x = -f_x$$
$$\partial_s n_y = -f_y$$
$$\partial_s m = n_y \cos\theta - n_x \sin\theta$$

with f the external force (per unit width) distributed along the beam. Here the only external force is gravity (with buoyancy taken into account), thus $f_y = 0$ and $f_x = (\rho_s - \rho_w)gt$. We therefore integrate between 0 and s the first two equations:

$$\begin{aligned} n_x(s) - n_x(0) &= -(\rho_s - \rho_w)gts \\ n_y(s) - n_y(0) &= 0 \end{aligned}$$

At $s = 0$ there is an upward vertical force F (per unit width) so that $n_y(0) = 0$ and $n_x(0) = F$. So finally:

$$\begin{aligned} n_x(s) &= F - (\rho_s - \rho_w)gts \\ n_y(s) &= 0 \end{aligned}$$

We insert these results into the internal moment equation and consider the film slender enough that its local moment is proportional to the local curvature $m(s) = B\partial_s\theta(s)$, with B the bending modulus of the beam (equivalent to that of the elastic film measured experimentally, which makes up a single side of the fold). We obtain the equation describing the shape of the beam:

$$\partial_s m = B\partial_s^2\theta = -[F - (\rho_s - \rho_w)gts]\sin\theta$$

The boundary conditions $\partial_s\theta(s = 0) = 0$, $\theta(s = L^*) = 0$ are imposed. The system is made dimensionless by dividing s by L^*:

$$\begin{aligned} \partial_s^2\theta + \left[\widetilde{F} - \left(\frac{L^*}{\ell_g}\right)^3 s\right]\sin\theta = 0 \\ \partial_s\theta(s = 0) = 0, \quad \theta(s = 1) = 0 \end{aligned} \tag{6}$$

$\widetilde{F} = \frac{FL^{*2}}{B}$ is the dimensionless force and $\ell_g = \left(\frac{B}{(\rho_s - \rho_w)gt}\right)^{1/3}$ is the elasto-gravitational length which is the characteristic length at which the weight of the film is enough to cause it to bend.

To find the onset of buckling we consider small deformations and linearize equation (6) *i.e.* we let $\sin\theta \approx \theta$ giving

$$\partial_s^2\theta + \left[\widetilde{F} - \left(\frac{L^*}{\ell_g}\right)^3 s\right]\theta = 0$$

We introduce the new arclength variable $r = \frac{L^*}{\ell_g}\left(s - \widetilde{F}\left(\frac{\ell_g}{L^*}\right)^3\right)$, so that the equation becomes:

$$\partial_r^2\theta - r\theta = 0, \tag{7}$$

which has general solution

$$\theta(r) = C_1\,\mathrm{Ai}(r) + C_2\,\mathrm{Bi}(r) \tag{8}$$

with Ai and Bi the Airy functions of the first and second kind and the constants C_1 and C_2 are determined by the boundary conditions, which in the rescaled coordinates used here read

$$\partial_r\theta\left(r = -\widetilde{F}\left(\frac{\ell_g}{L^*}\right)^{2/3}\right) = 0, \quad \theta\left(r = \frac{L^*}{\ell_g}\left(1 - \widetilde{F}\left(\frac{\ell_g}{L^*}\right)^3\right)\right) = 0.$$

For non trivial solutions to exist ($\theta(s) \neq 0$, corresponding to buckling of the column) we need:

$$\begin{vmatrix} \mathrm{Ai}\left[\frac{L^*}{\ell_g}\left(1 - \widetilde{F}\left(\frac{\ell_g}{L^*}\right)^3\right)\right] & \mathrm{Bi}\left[\frac{L^*}{\ell_g}\left(1 - \widetilde{F}\left(\frac{\ell_g}{L^*}\right)^3\right)\right] \\ \mathrm{Ai}'\left[-\widetilde{F}\left(\frac{\ell_g}{L^*}\right)^2\right] & \mathrm{Bi}'\left[-\widetilde{F}\left(\frac{\ell_g}{L^*}\right)^2\right] \end{vmatrix} = 0$$

This equation is solved using `Mathematica`. The first root gives us the critical dimensionless force $\widetilde{F}_c$ to buckle (in mode 1) as a function of the dimensionless beam length (L^*/ℓ_g): $\widetilde{F}_c = \frac{F_c L^{*2}}{B} = \mathrm{f}\left((\frac{L^*}{\ell_g})^3\right)$ where the function f is found numerically.

In our experiment, it is the beam length L^* that is varied (the buoyancy force from the teardrop is constant). Since L^* appears in the non-dimensionalization of the force, it is more convenient to write:

$$\frac{F\ell_g^2}{B} = \left(\frac{\ell_g}{L_c}\right)^2 \mathrm{f}\left(\frac{L_c}{\ell_g}\right) \tag{9}$$

The predicted critical force, based on equation (9), is shown as the red curve in Fig. 6 of the main text. This qualitatively captures the fold's behaviour: there is a critical buoyancy force below which the fold never bends back towards the surface, regardless of the length L^*. However, the data points consistently lie well below the red curve described by (9). Using equation (5) of the main text, the lowest critical force ($F\ell_g^2/B \approx 1$) reduces to $M^{-2/3}(\frac{\mathscr{A}}{\ell_{eh}^2} - M\frac{\mathscr{L}}{\ell_{eh}}) \approx 1$. If we use images from the side to evaluate $\mathscr{A}/\ell_{eh}^2$ and $\mathscr{L}/\ell_{eh}$, we find that the critical dimensionless mass $M = 0.060$, which is below the experimentally determined value ($M \sim 0.14$). In most experiments the fold is not perfectly aligned with the vertical axis when it reaches self-contact (see, for example, Fig. 4(a) of the main text). The average angle α between the fold and the vertical axis is $|\alpha| = 10°$ (its maximum value is 26°).

To account for the effect of the slope of the fold at self-contact, we add an initial angle to the heavy hanging column model by changing the boundary condition at the top of the beam. We then solve equation (6) numerically with the new boundary condition $\theta(s = 1) = \alpha$ to get the beam shape. With an initial angle the transition from straight to a buckled configuration becomes smooth. We therefore need to define a criterion to describe the critical length L_c^*/ℓ_g for buckling. Here, we use the normalized free end horizontal displacement, $y/L^*(s = 0)$ (denoted as y_0), to give this criterion: when the beam is straight $y_0 = \sin(\alpha)$ but when the beam starts to bend y_0 increases (Fig. S3(a)). We define the critical length L_c^* as the length at which $y_0 - \sin(\alpha) > 0.1$. (This choice of threshold comes from experiments: the chosen threshold has to be much higher than the measurement uncertainty so that the "buckled" beam can be visually identified.)

Finally, we note that the force used in Fig. 6 of the main text is, in fact, an under-estimate of the true force (since the shape of the teardrop is measured from the side where surface tension plays an important role). We have shown in Fig. S2 (b) that away from the side the shape of the fold up to self-contact can be fitted by the solution in ref[4,5]. The width averaged force due to the encapsulated fluid is thus better estimated with the solution from ref[4,5] at self-contact. Fig. S3(b) therefore shows the phase diagram for the fold bending using the calculated values of the teardrop shape at self-contact, instead of that measured from side images. We find a good quantitative agreement with the tilted heavy hanging column model despite the numerous approximations. Moreover, the critical dimensionless mass is now $M = 0.094$, closer to the experimental value ($M \sim 0.14$).

5 Film characterization

Table S1 shows the densities and thicknesses of the films used in our experiments.

We use a tensile test to measure the Young's moduli and Poisson ratios of the materials used. In particular, the Young's modulus is extracted from a linear fit of the true stress as a function of the longitudinal strain, while the Poisson ratio is measured from the lateral strain as a function of the longitudinal strain. We find for the pure VPS dogbone that $\nu = 0.46$ and $E = 1.03$ MPa while for a dogbone of VPS with iron powder $\nu = 0.49$ and $E = 2.88$ MPa. The difference in Poisson ratio is not significant and we take the value $\nu = 0.5$ for all our films. However, the Young's modulus increases significantly as iron powder is added.

We also check that the values of the Young's modulus from the tensile tests are consistent with a beam deflection test on two films: one made of pure VPS $\rho_s = 1.20\ \mathrm{g\,cm^{-3}}$, the other one made of VPS mixed with iron powder $\rho_s = 2.39\ \mathrm{g\,cm^{-3}}$. We clamp the film horizontally and let a length L hang freely under its own weight. In this configuration the deflection at the end of the sheet is given by $y_{end} = \rho_s t L^4 g/(8B) = 3(1-\nu^2)\rho_s g L^4/(2Et^2)$. We extract E from a linear fit of y_{end} as a function of L^4, obtaining $E = 1.46 \pm 0.24$ MPa for the pure VPS film and $E = 2.56 \pm 0.47$ MPa for the film made of VPS with iron powder.

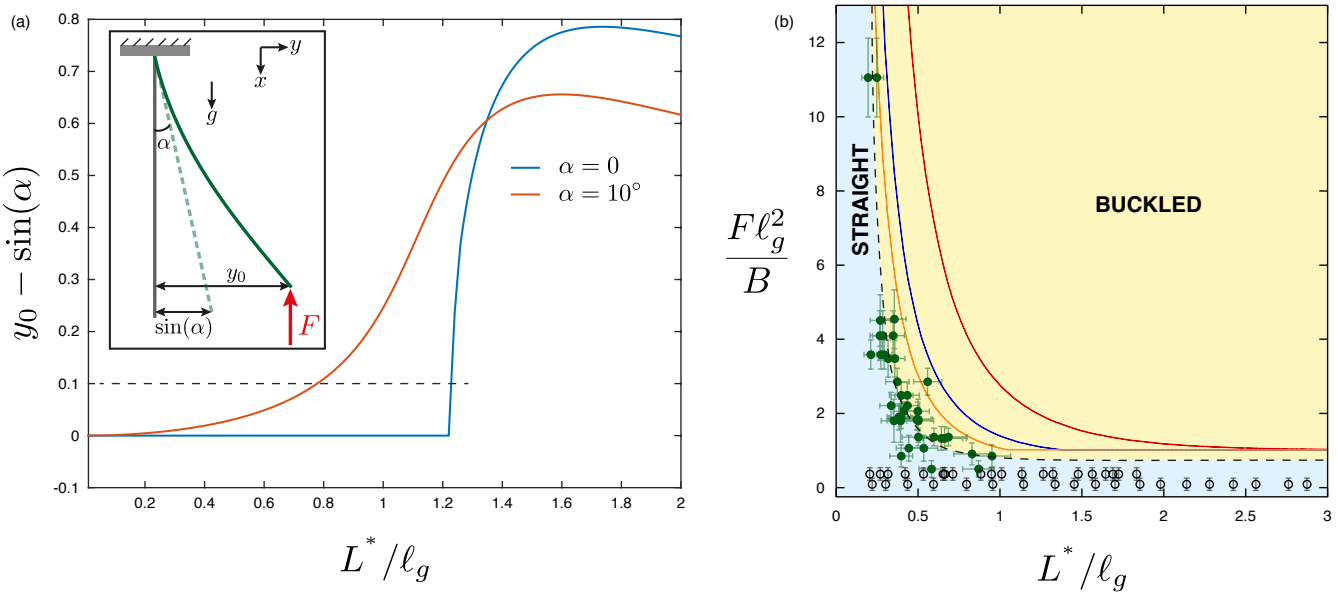

Figure S3: **(a)** Dimensionless horizontal end displacement of the beam as a function of its length for a dimensionless force $F\ell_g^2/B = 2$ with two different clamping angles at the end, α: $\alpha = 10°$ (orange curve) and $\alpha = 0°$ (blue curve). The horizontal dashed line shows our criterion for determining the critical buckling length L_c^*. *Inset* Schematic of the tilted heavy hanging column defining the horizontal end displacement y_0, with all lengths normalized by L^*. **(b)** Phase diagram of the post self-contact fold buckling using the solution of Diamant and Witten [1] to compute the teardrop area and perimeter. Green filled circles give the critical length L^* before buckling for each experiment. Black open circles represent experiments in which the fold never buckled. All parameters are varied in the data presented. The black dashed curve and background colours are guides for the eye to distinguish experimental phases. The red solid curve is the analytical result of the heavy hanging column theory (9), the blue (respectively orange) solid curve are the numerical results of the heavy hanging column theory with an initial angle of 10° (respectively 20°).

ρ_s ($\mathrm{g\,cm^{-3}}$)	W (mm)	L (mm)	t_{weight} (μm)	t_{laser} (μm)	$M_{air/water}$	$M_{oil/water}$
1.20	50	75	74 ± 6	54 ± 4	0.007 ± 0.001	0.030 ± 0.004
1.40	50	75	81 ± 5	90 ± 11	0.023 ± 0.004	0.100 ± 0.019
1.40	60	90	89 ± 4	89 ± 14	0.023 ± 0.005	0.091 ± 0.020
1.54	50	75	73 ± 4	79 ± 11	0.026 ± 0.005	0.104 ± 0.021
1.54	60	90	89 ± 4	109 ± 12	0.031 ± 0.005	0.131 ± 0.022
1.78	50	75	79 ± 4	78 ± 6	0.039 ± 0.005	0.144 ± 0.020
1.78	60	90	90 ± 4	98 ± 9	0.045 ± 0.007	0.178 ± 0.026
2.00	50	75	85 ± 4	92 ± 10	0.051 ± 0.008	
2.00	60	90	91 ± 3	104 ± 7	0.054 ± 0.007	
2.12	50	75	83 ± 3	99 ± 12	0.058 ± 0.01	
2.12	60	90	94 ± 3	117 ± 28	0.061 ± 0.018	
2.36	50	75	64 ± 3	80 ± 8	0.059 ± 0.009	
2.36	60	90	63 ± 2	70 ± 6	0.060 ± 0.009	
2.55	50	75	49 ± 2	64 ± 7	0.078 ± 0.013	
2.55	60	90	55 ± 2	69 ± 5	0.077 ± 0.010	

Table S1: Film properties. The values of M displayed are calculated using $M = 2\pi(\rho_s - \rho_w)t_{laser}/(\Delta\rho\lambda)$.

References

[1] H. Diamant and T. A. Witten, *Phys. Rev. Lett.*, 2011, **107**, 164302.

[2] O. Oshri, F. Brau and H. Diamant, *Phys. Rev. E*, 2015, **91**, 052408.

[3] L. Pocivavsek, R. Dellsy, A. Kern, S. Johnson, B. Lin, K. Y. C. Lee and E. Cerda, *Science*, 2008, **320**, 912–916.

[4] H. Diamant and T. A. Witten, *Phys. Rev. E*, 2013, **88**, 012401.

[5] M. Rivetti, *C. R. Mecanique*, 2013, **341**, 333–338.

[6] M. Rivetti and S. Neukirch, *J. Mech. Phys. Solids*, 2014, **69**, 143–155.

[7] J. Huang, B. Davidovitch, C. D. Santangelo, T. P. Russell and N. Menon, *Phys. Rev. Lett.*, 2010, **105**, 2–5.